BNL-113846-2017-JA

In-situ Visualization of State-of-Charge Heterogeneity within a LiCoO2 Particle that Evolves upon Cycling at Different Rates

Yahong Xu, Enyuan Hu, Kai Zhang, Xuelong Wang, Valery Borzenets, Zhihong Sun, Piero Pianetta, Xiqian Yu, Yijin Liu, Xiao-Qing Yang, Hong Li

Submitted to ACS Energy Letters

May 2017

Chemistry Department

Brookhaven National Laboratory

U.S. Department of Energy
USDOE Office of Science (SC),
Basic Energy Sciences (BES) (SC-22)

DISCLAIMER

In-situ Visualization of State-of-Charge Heterogeneity within a $LiCoO_2$ Particle that Evolves upon Cycling at Different Rates

Yahong Xu[Π,§,†], Enyuan Hu[#,†], Kai Zhang[‡,†], Xuelong Wang[£], Valery Borzenets[§], Zhihong Sun[Π], Piero Pianetta[§], Xiqian Yu[£,*], Yijin Liu[§,*], Xiao-Qing Yang[#,*], Hong Li[£]

Π College of Mechanical Engineering, Donghua University, Shanghai 200051, China

§ Stanford Synchrotron Radiation Lightsource, SLAC National Accelerator Laboratory, Menlo Park, CA 94025, USA

Chemistry Division, Brookhaven National Laboratory, Upton, NY 11973, USA

‡ Beijing Synchrotron Radiation Facility, Institute of High Energy Physics, Chinese Academy of Science, Beijing 100049, China

£ Beijing National Laboratory for Condensed Matter Physics, Institute of Physics, Chinese Academy of Sciences, Beijing 100190, China

ABSTRACT: For designing new battery systems with higher energy density and longer cycle life, it is important to understand the degradation mechanism of the electrode material, especially at the individual particle level. Using *in-situ* transmission X-ray microscopy (TXM) coupled with a pouch cell setup, the inhomogeneous Li distribution as well as the formation, population and evolution of inactive domains in a single $LiCoO_2$ particle were visualized as it was cycled for many times. It is found that the percentage of the particle that fully recovered to the pristine state is strongly related to the cycling rate. Interestingly, we also observed the evolution of the inactive region within the particle during long term cycling. The relationship between morphological degradation and chemical inhomogeneity, including formation of unanticipated Co metal phase, are also observed. Our work highlights the capability of *in-situ* TXM for studying the degradation mechanism of materials in LIBs.

TOC figure:

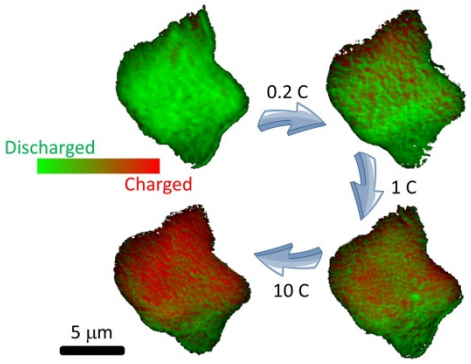

Lithium ion batteries (LIBs) are currently dominating the energy storage market. However, to expand their applications to other systems, such as electric vehicles and/or smart grid systems, significant improvements of their electrochemical performance are required in several aspects[1-4]. Generally, the capacity and sometimes also the voltage fade upon cycling. To address this issue, it is crucial to understand the fundamental degradation mechanisms of the electrode. In the past years, lots of research efforts have been directed toward this goal with much knowledge gained. Several degradation mechanisms have been observed, such as irreversible phase transition during cycling[5-6], loss of electric contact due to formation of cracks[7-8], and reduction of the transition metal cations due to oxygen loss etc[9-10]. While these studies are very informative and important, they are usually based on ensemble techniques such as X-ray diffraction, spectroscopy and electrochemical measurements (e.g. electrochemical impedance spectroscopy) that provide statistical information. A deeper and more fundamental insight would require observation at the individual particle or sub-particle level as have been emphasized by several previous works. For example, Yan *et al.* identified intragranular rather than intergranular cracking as the critical barrier for high-voltage usage of layer-structured cathode by using advanced scanning transmission electron microscopy (STEM)[11]. Lin *et al.* used atomic-scale scanning transmission electron microscopy (STEM) and electron energy loss spectroscopy (EELS)to study $LiNi_{0.4}Mn_{0.4}Co_{0.18}Ti_{0.02}O_2$ and observed the formation of rock salt phase on the surface, which leads to impedance and, consequently, capacity fade[12]. Xu *et al.* used transmission X-ray microscopy

(TXM) to investigate the electrochemical reaction induced morphological and chemical changes in the Li-rich $Li_2Ru_{0.5}Mn_{0.5}O_3$ cathode particles at the meso to nano scale, suggesting that both morphology and chemical heterogeneity play a key role in the capacity fade of this material[13].

Study of degradation mechanisms of cathode electrode materials in LIBs inevitably requires comparing the experimental data as a function of the state of charge (SOC) and/or the number of cycles. In many microscopic studies, different particles are chosen at different SOCs and from different cycles due to the lack of capability to keep tracking the same particle over multiple charge-discharge cycles, causing some arbitrariness to the data and making comparison more difficult. More recently, *in-situ* and *operando* X-ray microscopy has been demonstrated for study of LIBs through working with specifically designed coin cell[14-15], pouch cell[16], capillary cell[17], and liquid flowing cell[18]. However, due to practical challenges, these studies are usually limited to relatively short cycling history (within the first few cycles). In this work, a new type of *in-situ* pouch cell setup was designed for tracking and studying selected electrode particles over many cycles. Layered material $LiCoO_2$ was chosen for this study to avoid any structural complexities (e.g. cation disorder arising from transition metal and Li exchanging site in Ni-containing layered materials)[19-20] or any structural ambiguities (e.g. whether it is solid solution or composite for Li-rich materials)[6, 21-22]. $LiCoO_2$ is also technologically important because it possesses the highest theoretic density and packing density among the commercially available cathode materials. In commercial applications, $LiCoO_2$ currently allows the repeated extracting and inserting about 0.5 Li^+ per formula, giving a specific capacity of 140 mAh g^{-1}. To achieve higher capacity, one must charge this material to a higher cut-off voltage to utilize part of the other 0.5 Li per formula. Unfortunately, such practice would lead to a significant capacity fade.[23-26] To unravel the degradation mechanisms of $LiCoO_2$ when operated over a voltage range of 3V to 4.6V, *in-situ* transmission X-ray microscopy (TXM) is used here to visualize the $LiCoO_2$ particle's response under various cycling conditions. A rate-dependent chemical heterogeneity within the particle is clearly observed. The redistribution of inactive domains within the particle was also observed upon long term cycling. In addition, unanticipated metallic Co particle was found in the cycled cell, suggesting that the dissolution and precipitation of the Co is accompanied by the reduction of the cation. Our experimental result shows that the sub-particle level interplays of different chemical species strongly depend on the electrochemical environment, which is governed by the cycling rate and history. This work highlights the power and value of *in-situ* method for investigating the effects of cycling history at microscopic scale, which is relevant to the studies of many other battery materials and systems.

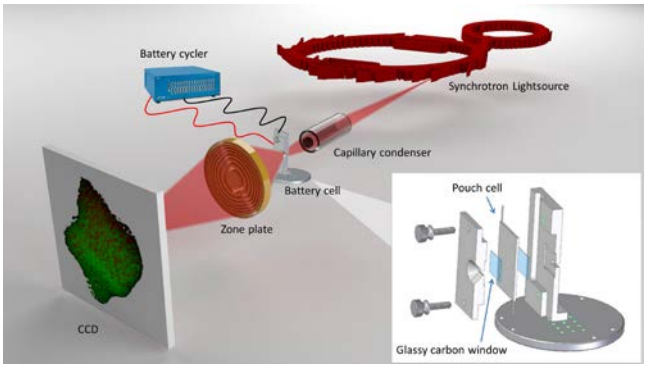

Figure 1. Schematic drawing of the setup used for in-situ spectro-microscopic study of LIBs (not to scale). The lower right inset shows a detailed view of the developed battery pouch cell system that allowed the *in-situ* study of $LiCoO_2$ particle's long term cycling behavior.

Before the *in-situ* TXM measurements (setup shown in Figure 1), *ex-situ* electrode powder recovered at the discharged state (at 3V) and the charged state (at 4.6V) were studied at the same beamline to acquire the signature spectra associated with these two extreme SOCs. These *ex-situ* samples were prepared with very slow cycling rate to ensure the phase purity. These two spectra (Supplementary Figure S1) were used to perform linear combination fitting of the *in-situ* XANES imaging data. We note here that we are not implying a two-phase transition for the reaction occurring in $LiCoO_2$ system, which could actually be rather complicated involving several intermediate and even metastable phases[24, 27-28]. For simplicity, only the fully charged state (at 4.6V) and the discharged state (at 3V) were studied in our *in-situ* experiment.

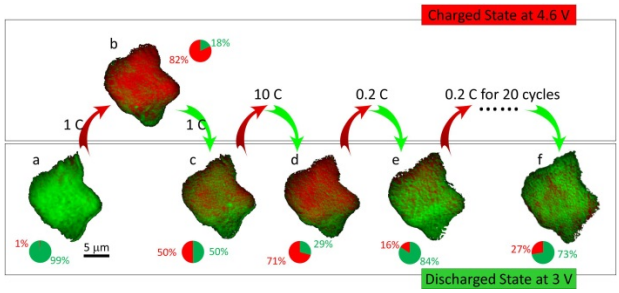

Figure 2. *In-situ* monitoring of the chemical heterogeneity in a single particle of $LiCoO_2$ up to 20 cycles. Panel (a) is the chemical map of the particle at its pristine state; panel (b) is at the charged state (at 4.6V); panels (c) through (e) are the chemical maps at discharged state (at 3V) after the particle went through cycles of different rates at 1C, 10C and 0.2C, respectively; panel (f) is the map at the discharged state after 20 cycles at 0.2C. All the chemical maps are color coded to the corresponding pie charts. The red area represents the domains at charged state and the green area represents the domains at discharged state.

As shown in Figure 2, the chemical change in a selected Li_xCoO_2 particle was monitored as the cell was cycled many times. At the pristine state, nearly the entire particle shows the discharged state ($LiCo^{3+}O_2$), which is color coded to green (Figure 2.a). Majority of this particle turned to the charged state (red) when the cell was charged to 4.6V at a rate of 1C (nC is the current required to either charge or discharge the electrode fully in 1/n hours) as shown in Figure 2.b. After the cell was discharged to 3V at a rate of 1C, only about 50% of this particle recovered to the discharged state (Figure 2.c). Due to the scope of research interest of this work, in the following experiment particle was scanned only at the discharged state. The portion of the particle that returned to the discharged state (green) is clearly dependent on the cycling rate as suggested by the chemical maps in Figures 2.d for 10C and 2.e for 0.2C. The cell was then cycled for 20 times at 0.2C for investigating the particle's response to stabilized and repeated reaction conditions (Figure 2.f). More details about the spectrum fitting and chemical map composing can be found in other publications[29] as well as the Supplementary Figure S2. The reason for the reaction heterogeneity of $LiCoO_2$ at high charging voltage could be due to the nucleation process (formation of the delithiated phase) that will be affected by the defects in the particle, and this is very likely a non-equilibrium process and therefore is rate dependent. It is noted that the electrochemical behavior of this particular particle may not be able to represent that of the whole cell as the bulk scale behavior could be different (Supplementary Figure S3). This is because the total amount of active

material in this cell is many orders of magnitude greater than the mass of the studied individual particle. However, this particular active particle allowed us to study the trend of the local chemical reaction's cycling rate dependency, which is critical to understand the fundamental degradation mechanism.

A few very interesting conclusions can be drawn from the chemical maps in Figure 2. First of all, memory effect was not observed in this particle. The pouch cell first went through cycles with relatively higher C rate, resulting in low recovery rate at 50% and lower (Figures 2.c and 2.d). However, the following low C rate cycles brought the recovery rate back to a higher level (Figures 2.e and 2.f).

To evaluate the rate dependency, the data was re-sorted and the particle's recovery rate at 3V discharged state was plotted as a function of the C rate. As shown in Supplementary Figure S4, the cycling rate is clearly negatively correlated with the particle's recovery rate. Further cycling at 0.2C for up to 20 cycles degraded the recovery rate from 84% to 73%, which, however, is still significantly higher than the high C rate circumstances. The degraded cycle performances is very likely due to the structural changes upon extended lithium extraction, which causes accumulation of irreversible structural (e.g. structural damage) and morphological changes (e.g. crack).

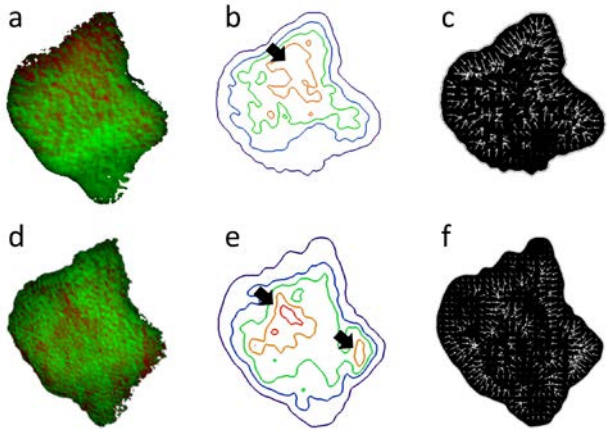

Figure 3. The chemical maps of the particle after the first cycle of 0.2C and the 20th cycle of 0.2C. Panels (a) and (d) are the same maps shown in Figures 2.e and 2.f; panels (b) and (e) are the contour maps of the material that failed to return to discharged state at OCV of 3V; panels (c) and (f) are the corresponding local chemical gradient maps, with the arrows indicating the direction and amplitude of the local chemical gradient.

For more detailed study of the particle's behavior when it is subjected to repeated and stabilized operating conditions, the chemical maps retrieved from the 1st and the 20th cycle of 0.2C were analyzed in more details. As shown in the contour maps of the material that failed to return to discharged state at OCV of 3V (Figures 3.b and 3.e), the redistribution of the inactive domain was clearly observed. It evolved from a single hot zoon (black arrow in Figure 3.b) to two hot spots (black arrows in Figure 3.e), suggesting that the so-called inactive domain still has some Li-ion mobility that allows the Li to be rearranged within the particle. The chemical gradient maps (Figures 3.c and 3.f, in which the white arrows indicate the direction and amplitude of the chemical gradient) also displayed significant differences. When the particle was cycled at 0.2C for the 1st time, large chemical gradient occurs at the upper edge of the particle. It might be caused by the inhomogeneous electronic contact and/or electrolyte wetting and could be an away-from-equilibrium effect. Due to repeated electrochemistry activation process, the chemical gradient map changed. The large chemical gradients in Figure 3.f are clearly associated with the two hot spots highlighted in Figure 3.e, indicative of nucleation of inactive phases, suggesting barriers within the particle that prevents free transportation of Li.

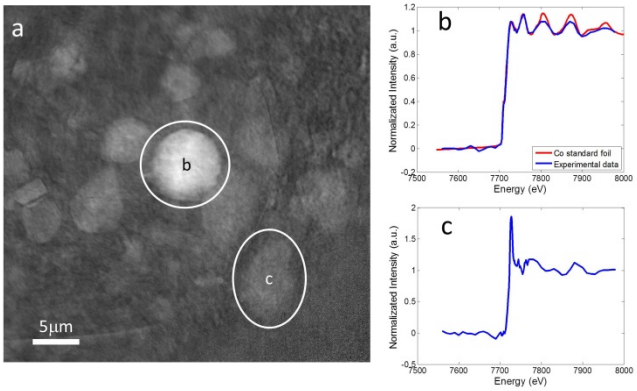

Figure 4. Metallic Co particle formed upon cycling of the cell. Panel (a) is a transmission x-ray image at a selected location on the pouch cell. Panels (b) and (c) are retrieved spectra over the two selected particle labeled accordingly on panel (a). When compared to the spectrum of pure Co foil (red curve in (b)), the particle at the center of the image clearly shows metallic Co signature, while the spectrum in panel (c) is a very typical signature of Li_xCoO_2.

Another very interesting phenomenon is that some metallic Co particles are formed after the cycling sequence. We applied an unsupervised data mining method known as DBSCAN[30] to evaluate the large spectro-microscopic data of over 100 individual particles acquired as we surveyed the pouch cell after the cycling sequence. Particles with distinct chemical finger prints are identified automatically as "outliers". Although many of those "outliers" are simply data points too noisy to be meaningful, one of the automatically identified particles (Figure 4) clear shows spectroscopic signature of metallic Co. Since the cell was operated between 3V and 4.6V with no deep discharging history, direct electrochemical reduction of Co^{3+} to metallic Co is highly unlikely. The formation of metallic Co particle is attributed to the dissolution and precipitation of Co cations, which is a vital mechanism that affects the overall performance of $LiCoO_2$ as well as other layered transition metal oxide materials[31-33]. Our experiment provides the direct evidence for the dissolution and precipitation of transition metal ions within real cells. It highlights the importance of surface coating to improve electrochemical performances of the layered cathode materials. More detailed descriptions of the data mining aspect of this work will be reported separately in a following manuscript.

In-situ 2D nanoscale XANES imaging provides valuable insight into the rate dependent degradation mechanism of the $LiCoO_2$ electrode, however, we lack direct evidence about the relationship between the morphological and the chemical degradation due to the fact that the 2D measurements cannot resolve the depth information. To supplement our *in-situ* study described above, we performed *ex-situ* 3D XANES[34-35] study of a selected particle recovered from a cell that was cycled at 0.2 C and was disassembled at the discharged state. As shown in the 3D rendering of the chemical distribution within the studied particle (Figure 5), only a small region on the surface remained at the charged state (red). We clearly see a crack, as highlighted by the circle in Figure 5.b, which is associated with the inactive domain (red), suggesting the close relationship between the morphological degradation and the chemical inhomogeneity.

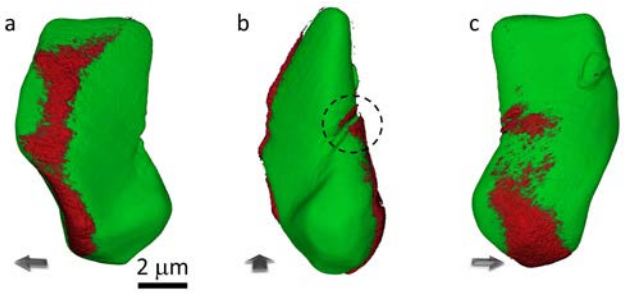

Figure 5. *Ex-situ* 3D chemical map of a selected particle recovered from a cell that was cycled at 0.2C and disassembled at OCV of 3V. Panels a, b and c are the same particle in different viewing angles as indicated by the arrows on the bottom. The chemical components are color coded in the 3D rendering with the discharged state shown in green and the charged state shown in red (the portion of the particle that failed to return to the discharged state at OCV of 3V).

In summary, 2D mapping of chemical heterogeneity of $LiCoO_2$ particle in operating conditions was performed by using a novel design of *in-situ* setup that enabled tracking the cycling history of single active particle. The same particle was followed for many cycles to conduct a systematic study of the rate dependency of the particle's recovery rate at a specific SOC (3V here). A strong negative correlation between the particle's recovery rate and the cycling C rate was observed. After 20 cycles at 0.2C, the redistribution of the inactive domain at sub-particle level was clearly observed indicating the particle's ability to re-adjust itself in response to repeated and stabilized reaction conditions. After the designed cycling sequence, we observed the formation of unanticipated metallic Co particles. This phenomenon is attributed to the dissolution and precipitation of Co cations. In addition, *ex-situ* 3D chemical mapping of a selected $LiCoO_2$ particle shows that a crack was closely associated with the inactive domain suggesting close relationship between the morphological degradation and the chemical inhomogeneity. A better design of $LiCoO_2$ requires conformal coating to prevent the dissolution of the Co cations. Uniform electronic wiring of the electrode is also crucial to realize homogenous de/lithiation. The insight we gathered from the presented study is relevant to the design of other layered transition metal cathode materials. Furthermore, this article illustrates transmission X-ray microscopy (TXM) a pivotal tool to probe the morphological and chemical evolution on particle and electrode scale.

EXPERIMENTAL METHODS

X-ray transparent *in-situ* battery pouch cells were specifically designed for this experiment. The cells are composed of a lithium metal anode, a Celgard separator soaked in an electrolyte of $LiPF_6$ (1 M) in ethylene carbonate and dimethyl carbonate (volume ratio 1:1), and a cathode of micrometer-sized $LiCoO_2$ (80 wt%; Alfa Aesar), carbon black (10 wt%; Chevron) and Polyvinylidene fluoride (10 wt%; Kureha). SEM and XRD characterization of the pristine material is presented in Supplementary Figure S5. To prepare the electrode, $LiCoO_2$ powder was mixed with carbon black and poly-vinylidene fluoride in N-methylpyrrolidone solvent to make a slurry. Then it was coated on Al foil. In order to avoid the overlap of the particles in the path of X-ray beam for collecting X-ray images, the loading amount of the active material on current collector is very small (around 0.2mg/cm^2). The electrodes were dried under vacuum at 120 °C for 24 h, and then the cells are assembled inside an argon-filled glovebox and heat-sealed in polyester pouches with aluminum and copper current collectors for cathode and anode electrodes, respectively.

We conducted *in-situ* TXM imaging on the cell described above using a configuration shown in Figure 1. The cell holder has two glassy carbon windows, each at 500 microns thick, providing sufficient pressure while allowing X-ray transmission rate of about 50% at the working energy. The typical exposure time for single image is 1 second or less. The pouch cell holder is designed to be asymmetric with the X-ray transparent window located on the edge to minimize the travel distance from the particle of interest to the open space, where the background images are acquired. Nominal spatial resolution of our TXM measurement is at 30.4 nm. However, due to difficulties associated with spatial registration of images with noise, we make conservative estimation of effective spatial resolution at 3 by 3 pixels (~90 nm). More details of the synchrotron beamline configuration and the concept of TXM spectro-microscopy can be found elsewhere[35-36].

In the spectro-microscopic scan, the energy of the incident X-rays is scanned from 7560 eV to 7980 eV with 105 energy points recorded. Over the near edge region (7700 eV to 7770 eV), we choose the energy step at 1 eV to ensure sufficient energy resolution. The pre-edge and post edge regions were scanned with energy steps of 10 eV to cover a relatively wide energy window for normalization of the spectra. While the total amount of time needed for such a scan is about 30 minutes, more than 90 percent is due to the motor movement. As a result, no obvious radiation damage effect was observed in our experiment, as indicated by the fact that the particle of interest was still active after more than 20 cycles.

ASSOCIATED CONTENT

AUTHOR INFORMATION

Corresponding Author

* liuyijin@slac.stanford.edu

* xyu@iphy.ac.cn

* xyang@bnl.gov

Author Contributions

Y. Liu and X. Yu designed the work. V. Borzenets, Y. Liu, X. Yu and P. Pianetta designed the in-situ battery setup. X. Wang and X. Yu did the characterization of the pristine material and prepared the battery pouch cell. Y. Xu, E. Hu, X. Yu and Y. Liu performed the TXM measurements. Y. Xu, E. Hu, K. Zhang, X. Yu, Y. Liu analyzed the data. Z. Sun, P. Pianetta contributed to the interpretation of the spectro-microscopy data. Y. Xu, E. Hu, K. Zhang, X. Yu and Y. Liu prepared the manuscript with critical inputs from all the authors. X.-Q. Yang and H. Li reviewed and finalized the manuscript.

†These authors equally contributed to this work.

Notes

The authors declare no competing financial interest.

ACKNOWLEDGMENT

The support from D. Van Campen, D. Day, and R. Davis for the experiments at beamlines 6-2C and 4-1 of SSRL is gratefully acknowledged. This research used beam line 8-ID of the National Synchrotron Light Source II, a U.S. Department of Energy (DOE) Office of Science User Facility operated for the DOE Office of Science by Brookhaven National Laboratory under Contract No. DE-SC0012704. The work at IOP was supported by funding from

Ministry of Science and Technology of China (Grants 2016YFB0100300). The work at Brookhaven National Laboratory was supported by the U.S. Department of Energy, the Assistant Secretary for Energy Efficiency and Renewable Energy, Office of Vehicle Technologies through Advanced Battery Material Research (BMR) program (Battery500 consortium) under Contract No. DE-SC0012704. This work was partly supported by the National Key Research and Development Program of China (Grant No. 2016YFA0400900), the National Natural Science Foundation of China (Grant No. 11535015, U1632110). Portion of this work is supported by Open Research Foundation of State Key Lab. of Digital Manufacturing Equipment & Technology in Huazhong University of Science & Technology. Use of the Stanford Synchrotron Radiation Lightsource, SLAC National Accelerator Laboratory, is supported by the U.S. Department of Energy, Office of Science, Office of Basic Energy Sciences under Contract No. DE-AC02-76SF00515.

Supporting Information Available: Supplementary figures S1 to S5 present hard X-ray absorption spectrums of the electrode, battery performance test, SEM, and XRD results.

REFERENCES

(1)Tarascon, J. M.; Armand, M. Issues and challenges facing rechargeable lithium batteries. *Nature* **2001**, *414*, 359-367.

(2)Goodenough, J. B.; Kim, Y. Challenges for Rechargeable Li Batteries. *Chem. Mater.* **2010**, *22*, 587-603.

(3)Goodenough, J. B.; Park, K. S. The Li-Ion Rechargeable Battery: A Perspective. *J. Am. Chem. Soc.* **2013**, *135*, 1167-1176.

(4)Whittingham, M. S. Lithium batteries and cathode materials. *Chem. Rev.* **2004**, *104*, 4271-4301.

(5)Chen, C. J.; Pang, W. K.; Mori, T.; Peterson, V. K.; Sharma, N.; Lee, P. H.; Wu, S. H.; Wang, C. C.; Song, Y. F.; Liu, R. S. The Origin of Capacity Fade in the $Li_2MnO_3{\cdot}LiMO_2$ (M = Li, Ni, Co, Mn) Microsphere Positive Electrode: An Operando Neutron Diffraction and Transmission X-ray Microscopy Study. *J. Am. Chem. Soc.* **2016**, *138*, 8824-8833.

(6)Gu, M.; Belharouak, I.; Zheng, J. M.; Wu, H. M.; Xiao, J.; Genc, A.; Amine, K.; Thevuthasan, S.; Baer, D. R.; Zhang, J. G.; Browning, N. D.; Liu, J.; Wang, C. M. Formation of the Spinel Phase in the Layered Composite Cathode Used in Li-Ion Batteries. *ACS Nano* **2013**, *7*, 760-767.

(7)Li, J. C.; Zhang, Q. L.; Xiao, X. C.; Cheng, Y. T.; Liang, C. D.; Dudney, N. J. Unravelling the Impact of Reaction Paths on Mechanical Degradation of Intercalation Cathodes for Lithium-Ion Batteries. *J. Am. Chem. Soc.* **2015**, *137*, 13732-13735.

(8)Zheng, J. M.; Gu, M.; Xiao, J.; Zuo, P. J.; Wang, C. M.; Zhang, J. G. Corrosion/Fragmentation of Layered Composite Cathode and Related Capacity/Voltage Fading during Cycling Process. *Nano Lett.* **2013**, *13*, 3824-3830.

(9)Hu, E. Y.; Lyu, Y. C.; Xin, H. L. L.; Liu, J.; Han, L. L.; Bak, S. M.; Bai, J. M.; Yu, X. Q.; Li, H.; Yang, X. Q. Explore the Effects of Microstructural Defects on Voltage Fade of Li- and Mn-Rich Cathodes. *Nano Lett.* **2016**, *16*, 5999-6007.

(10)Yu, X. Q.; Lyu, Y. C.; Gu, L.; Wu, H. M.; Bak, S. M.; Zhou, Y. N.; Amine, K.; Ehrlich, S. N.; Li, H.; Nam, K. W.; Yang, X. Q. Understanding the Rate Capability of High-Energy-Density Li-Rich Layered $Li_{1.2}Ni_{0.15}Co_{0.1}Mn_{0.55}O_2$ Cathode Materials. *Adv. Energy Mater.* **2014**, *4*, 1-11..

(11)Yan, P. F.; Zheng, J. M.; Gu, M.; Xiao, J.; Zhang, J. G.; Wang, C. M. Intragranular cracking as a critical barrier for high-voltage usage of layer-structured cathode for lithium-ion batteries. *Nat. Commun.* **2017**, *8*, 1-9.

(12)Lin, F.; Markus, I. M.; Nordlund, D.; Weng, T. C.; Asta, M. D.; Xin, H. L. L.; Doeff, M. M. Surface reconstruction and chemical evolution of stoichiometric layered cathode materials for lithium-ion batteries. *Nat. Commun.* **2014**, *5*, 1-8..

(13)Xu, Y. H.; Hu, E. Y.; Yang, F. F.; Corbett, J.; Sun, Z. H.; Lyu, Y. C.; Yu, X. Q.; Liu, Y. J.; Yang, X. Q.; Li, H. Structural integrity-Searching the key factor to suppress the voltage fade of Li-rich layered cathode materials through 3D X-ray imaging and spectroscopy techniques. *Nano Energy* **2016**, *28*, 164-171.

(14)Li, L. S.; Chen-Wiegart, Y. C. K.; Wang, J. J.; Gao, P.; Ding, Q.; Yu, Y. S.; Wang, F.; Cabana, J.; Wang, J.; Jin, S. Visualization of electrochemically driven solid-state phase transformations using operando hard X-ray spectro-imaging. *Nat. Commun.* **2015**, *6*,1-8..

(15)Yu, Y. S.; Kim, C.; Liu, Y. J.; van der Ven, A.; Meng, Y. S.; Kostecki, R.; Cabana, J. Nonequilibrium Pathways during Electrochemical Phase Transformations in Single Crystals Revealed by Dynamic Chemical Imaging at Nanoscale Resolution. *Adv. Energy Mater.* **2015**, *5*, 1402040-1402048.

(16)Nelson, J.; Misra, S.; Yang, Y.; Jackson, A.; Liu, Y. J.; Wang, H. L.; Dai, H. J.; Andrews, J. C.; Cui, Y.; Toney, M. F. In Operando X-ray Diffraction and Transmission X-ray Microscopy of Lithium Sulfur Batteries. *J. Am. Chem. Soc.* **2012**, *134*, 6337-6343.

(17)Wang, J. J.; Chen-Wiegart, Y. C. K.; Eng, C.; Shen, Q.; Wang, J. Visualization of anisotropic-isotropic phase transformation dynamics in battery electrode particles. *Nat. Commun.* **2016**, *7*,1-7.

(18)Lim, J.; Li, Y. Y.; Alsem, D. H.; So, H.; Lee, S. C.; Bai, P.; Cogswell, D. A.; Liu, X. Z.; Jin, N.; Yu, Y. S.; Salmon, N. J.; Shapiro, D. A.; Bazant, M. Z.; Tyliszczak, T.; Chueh, W. C. Origin and hysteresis of lithium compositional spatiodynamics within battery primary particles. *Science* **2016**, *353*, 566-571.

(19)Breger, J.; Dupre, N.; Chupas, P. J.; Lee, P. L.; Proffen, T.; Parise, J. B.; Grey, C. P. Short- and long-range order in the positive electrode material, $Li(NiMn)_{0.5}O_2$: A joint X-ray and neutron diffraction, pair distribution function analysis and NMR study. *J. Am. Chem. Soc.* **2005**, *127*, 7529-7537.

(20)Lee, J.; Urban, A.; Li, X.; Su, D.; Hautier, G.; Ceder, G. Unlocking the Potential of Cation-Disordered Oxides for Rechargeable Lithium Batteries. *Science* **2014**, *343*, 519-522.

(21)Yu, H. J.; Ishikawa, R.; So, Y. G.; Shibata, N.; Kudo, T.; Zhou, H. S.; Ikuhara, Y. Direct Atomic-Resolution Observation of Two Phases in the $Li_{1.2}Mn_{0.567}Ni_{0.166}Co_{0.067}O_2$ Cathode Material for Lithium-Ion Batteries. *Angew. Chem. Int. Ed.* **2013**, *52*, 5969-5973.

(22)Koga, H.; Croguennec, L.; Mannessiez, P.; Menetrier, M.; Weill, F.; Bourgeois, L.; Duttine, M.; Suard, E.; Delmas, C. $Li_{1.20}Mn_{0.54}Co_{0.13}Ni_{0.13}O_2$ with Different Particle Sizes as Attractive Positive Electrode Materials for Lithium-Ion Batteries: Insights into Their Structure. *J. Phys. Chem. C* **2012**, *116*, 13497-13506.

(23)Mizushima, K.; Jones, P. C.; Wiseman, P. J.; Goodenough, J. B. Li_xCoO_2 (0<xizushima, K.; Jones, P. C.; Wiseman, P. J.; Goodenough, J. B. y. *Mater. Res. Bull.* **1980**, *15*, 783-789.

(24)Amatucci, G. G.; Tarascon, J. M.; Klein, L. C. CoO_2, the end member of the Li_xCoO_2 solid solution. *J. Electrochem. Soc.* **1996**, *143*, 1114-1123.

(25)Cho, J.; Kim, Y. J.; Kim, T. J.; Park, B. Zero-strain intercalation cathode for rechargeable Li-ion cell. *Angew. Chem. Int. Ed.* **2001**, *40*, 3367-3369.

(26)Chen, Z. H.; Dahn, J. R. Improving the capacity retention of $LiCoO_2$ cycled to 4.5 V by heat-treatment. *Electrochem. Solid-State Lett.* **2004**, *7*, A11-A14.

(27)Chen, Z. H.; Lu, Z. H.; Dahn, J. R. Staging phase transitions in $LixCoO_2$. *J. Electrochem. Soc.* **2002,** *149*, A1604-A1609.

(28)Ohzuku, T.; Ueda, A. Solid-State Redox Reactions of $LiCoO_2$ (R-3m) for 4 Volt Secondary Lithium Cells. *J. Electrochem. Soc.* **1994**, *141*, 2972-2977.

(29)Liu, Y.; Andrews, J.; Meirer, F.; Mehta, A.; Gil, S. C.; Sciau, P.; Mester, Z.; Pianetta, P. Applications of Hard X-ray Full-Field Transmission X-ray Microscopy at SSRL, *AIP Conf. Proc.* **2011**, 1365, 357-360.

(30)Duan, X. Y.; Yang, F. F.; Antono, E.; Yang, W. G.; Pianetta, P.; Ermon, S.; Mehta, A.; Liu, Y. J. Unsupervised Data Mining in nanoscale X-ray Spectro-Microscopic Study of NdFeB Magnet. *Sci. Rep.* **2016**, *6*,1-8.

(31)Amatucci, G. G.; Tarascon, J. M.; Klein, L. C. Cobalt dissolution in $LiCoO_2$-based non-aqueous rechargeable batteries. *Solid State Ion.* **1996**, *83*, 167-173.

(32)Jeong, S.; Park, S.; Cho, J. High-Performance, Layered, 3D-$LiCoO_2$ Cathodes with a Nanoscale Co_3O_4 Coating via Chemical Etching. *Adv. Energy Mater.* **2011**, *1*, 368-372.

(33)Kim, Y. J.; Cho, J. P.; Kim, T. J.; Park, B. Suppression of cobalt dissolution from the $LiCoO_2$ cathodes with various metal-oxide coatings. *J. Electrochem. Soc.* **2003**, *150*, A1723-A1725.

(34)Liu, Y. J.; Wang, J. Y.; Azuma, M.; Mao, W. L.; Yang, W. G. Five-dimensional visualization of phase transition in BiNiO3 under high pressure. *Appl. Phys. Lett.* **2014**, *104*,1-8.

(35)Meirer, F.; Cabana, J.; Liu, Y. J.; Mehta, A.; Andrews, J. C.; Pianetta, P. Three-dimensional imaging of chemical phase transformations at the

nanoscale with full-field transmission X-ray microscopy. *J. Synchrotron Radiat.* **2011**, *18*, 773-781.
(36)Liu, Y. J.; Meirer, F.; Wang, J. Y.; Requena, G.; Williams, P.; Nelson, J.; Mehta, A.; Andrews, J. C.; Pianetta, P. 3D elemental sensitive imaging using transmission X-ray microscopy. *Anal. Bioanal. Chem.* **2012**, *404*, 1297-1301.